


# An in vitro assessment of atrial fibrillation flow types on cardiogenic emboli trajectory paths

Fiona Malone<sup>1</sup> , Eugene McCarthy<sup>1</sup>, Patrick Delassus<sup>1</sup>, Jan-Hendrick Buhk<sup>2</sup>, Jens Fiehler<sup>2</sup> and Liam Morris<sup>1</sup>

Proc IMechE Part H:  
*J Engineering in Medicine*  
2020, Vol. 234(12) 1421–1431  
© IMechE 2020  
Article reuse guidelines:  
sagepub.com/journals-permissions  
DOI: 10.1177/0954411920946873  
journals.sagepub.com/home/pih  


## Abstract

Atrial fibrillation is the most significant contributor to thrombus formation within the heart and is responsible for 45% of all cardio embolic strokes, which account for approximately 15% of acute ischemic strokes cases worldwide. Atrial fibrillation can result in a reduction of normal cardiac output and cycle length of up to 30% and 40%, respectively. A total of 240 embolus analogues were released into a thin-walled, patient-specific aortic arch under normal (60 embolus analogues) and varying atrial fibrillation (180 embolus analogues) pulsatile flow conditions. Under healthy flow conditions ( $n = 60$ ), the embolus analogues tended to follow the flow rate split through each outlet vessel. There was an increase in clot trajectories along the common carotid arteries under atrial fibrillation flow conditions. A shorter pulse period (0.3 s) displayed the highest percentage of clots travelling to the brain (24%), with a greater percentage of clots travelling through the left common carotid artery (17%). This study provides an experimental insight into the effect varying cardiac output and cycle length can have on the trajectory of a cardiac source blood clots travelling to the cerebral vasculature and possibly causing a stroke.

## Keywords

Atrial fibrillation, stroke, cardiogenic emboli, cardiac output, pulse period, embolus analogues, patient-specific models

Date received: 7 August 2019; accepted: 1 July 2020

## Introduction

Atrial fibrillation (AF) is the most common irregular heartbeat among the global population<sup>1</sup> and can be defined as an average reduction in normal cardiac output (CO) and pulse period or cycle length (CL) of up to 30% and 40%, respectively.<sup>2</sup> AF is an independent risk factor for thromboembolism in patients, and it is estimated that 15%–20% of acute ischemic strokes (AIS) occur in patients with AF. Approximately 35% of AF patients will experience stroke in their lifetime, and 15% or more will experience recurrent brain infarction within 1 year. The prevalence of AF, and risk of stroke, increases with age.<sup>3–5</sup>

The reduced blood flow velocity in the left atrium can result in the formation of emboli ranging in size from a few millimetres to 4 cm.<sup>6</sup> It is clear, AF is a contributing factor to blood clot formation and embolisation. However, it is unclear if the altered haemodynamic also influence the trajectory paths and ultimately the final lodgement locations of these emboli. AF has been shown to be related to a wide

spectrum of abnormal haemodynamics<sup>2,7–11</sup>; however, it is interesting to try and understand which elements of the altered haemodynamics, CO and/or CL, contribute more to the trajectory paths of cardiogenic emboli along the aortic arch and eventually towards the cerebral vasculature.

Embolitic blood clot trajectory paths have previously been modelled computationally and experimentally.<sup>12–17</sup> Bushi et al.<sup>12</sup> experimentally analysed trajectory paths of small particles in idealised bifurcation models. Fahy et al.<sup>14</sup> and Chung et al.<sup>13</sup> both analysed trajectory paths in Circle of Willis (CoW) models under healthy flow

<sup>1</sup>GMedTech, Department of Mechanical and Industrial Engineering, Galway-Mayo Institute of Technology, Galway, Ireland

<sup>2</sup>Department of Diagnostic and Interventional Neuroradiology, University Medical Center Hamburg-Eppendorf, Hamburg, Germany

## Corresponding author:

Fiona Malone, GMedTech, Department of Mechanical and Industrial Engineering, Galway-Mayo Institute of Technology, Galway H91T8NW, Ireland.

Email: fiona.malone@gmit.ie

conditions. However previous work completed has shown the limitations of the embolus analogues (EAs) used by both Fahy and Chung are not comparable with human EAs.<sup>15-17</sup> Both studies also only included the Circle of Willis in the anatomical models and not the aortic arch.

Carr et al.<sup>18</sup> demonstrated computationally that cardiogenic emboli appeared to have a strong size-destination relationship in 10 aortic arch models. Choi et al.<sup>19</sup> numerically assessed the trajectories of rigid, spherical particles within an idealised three-dimensional (3D) aortic arch model, comprising of three branching arteries under AF conditions. It was found that the reduced CO and CL significantly increased the incidence of embolisation to the brain that tended to travel more often through the left common carotid artery (LCCA). Previous experimental studies with varying aortic arches have verified this and have experimentally shown that AF can increase the propensity of stroke by up to 24% in certain physiological and anatomical circumstances.<sup>15,16</sup>

Given the variable nature of AF haemodynamics, experimentally identifying the roles an altered CO and CL can play in cardio embolic trajectory paths, may help clinicians understand better the embolic trajectory paths of blood clots that result in AIS. Obtaining clinical data, such as velocity profiles and physiological data surrounding AF, CO and CL, is very difficult.

Reducing a healthy CO up to 30% and CL up to 40% may be an introduction to investigate the effect altered haemodynamics have on embolic trajectory paths. There are currently no in vitro studies that examine the effect these cardiovascular reductions have on the trajectory paths of cardiogenic emboli within a patient-specific model. This study will provide a unique insight into the CO and CL and the parameters that influence a cardiac source blood clot to travel towards the head. The results from this work will go on to support future computational work in modelling AF and its effects on AIS.

## Materials and methods

### Model and rig

A medical image data set of the aortic arch of a Romanesque shape, which is present in over 80% of patients,<sup>20</sup> with Type II<sup>21</sup> branching configuration for a 77-year-old male case, with AF and a distal occlusion of the right M1 vessel, was obtained from the University Medical Centre Hamburg-Eppendorf (UKE), Germany. The commercially available, image reconstruction software, Mimics (Materialise, Leuven, Belgium) was used to generate a 3D mask, saved in STL format (see supplementary material), from the 2D medical image data set (Figure 1(a)) by applying various segmentation and smoothing methods.<sup>22</sup>

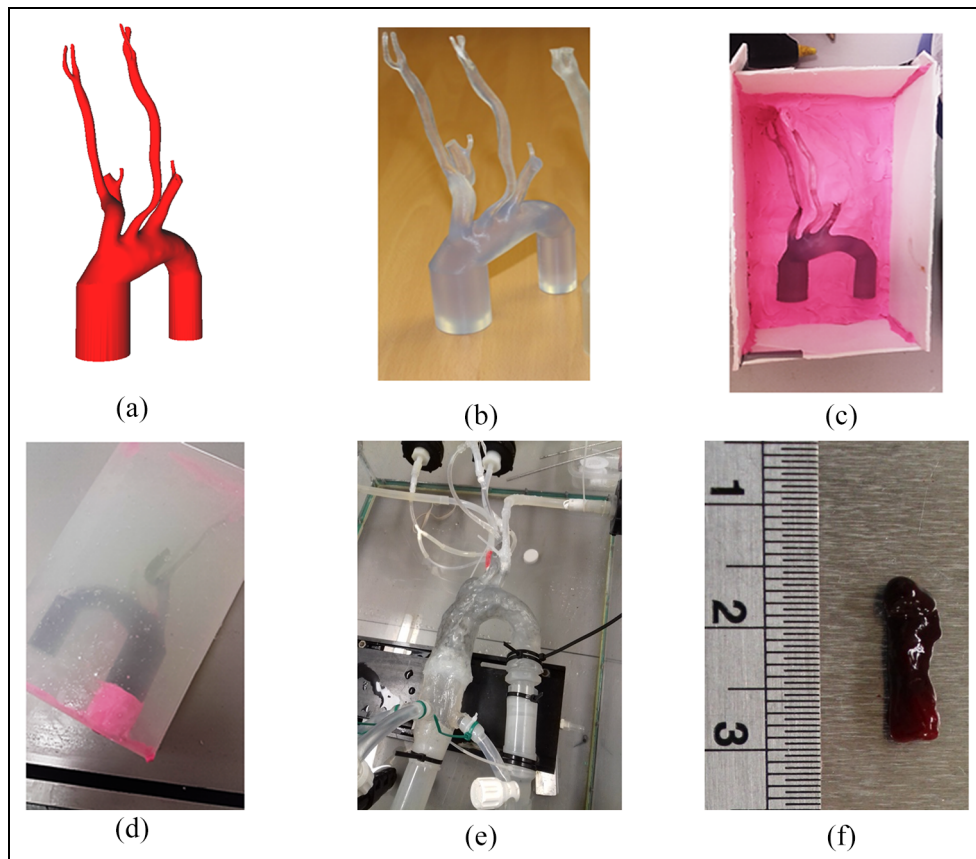


**Figure 1.** (a) 3D mask of 2D patient data set using Mimics (Materialise); (b) 3D printed geometry; (c and d) two-part mould; (e) flexible model in rig with three-way connector; and (f) bovine embolus analogue.

The aortic arch was 3D printed commercially (LPE 3D printing, Belfast, United Kingdom) (Figure 1(b)). A cast of the arch was made from a two-part silicone mould, using the 3D printed aortic arch as a solid core (Figure 1(c)). Once the silicone cured, the core was removed and a low melting point alloy (LMPA) was cast in the silicone mould to recreate the aortic arch geometry (Figure 1(d)). The Young's modulus of Elastosil 4641 silicone with Thivex silicone thickener (Wacker Chemie AG, Munich, Germany) was  $1.04 \pm 0.098$  MPa and was within the range for a typical aortic tissue.<sup>23–25</sup> The silicone mixture was painted onto the LMPA arch in layers to achieve a wall thickness of 2 mm, and 1.5 mm for the branching arches.<sup>24</sup> The LMPA was melted resulting in a flexible patient-specific aortic arch model (Figure 1(e)).

### Embolus Analogues

Bovine blood was obtained from a local abattoir (Burkes, Gort, Galway, Ireland) which is a European Union approved abattoir supervised by Galway County Council, Ireland, veterinary services. The mechanical properties of the blood clots (Figure 1(f)) were validated by in-house methods.<sup>26</sup> The bovine blood clots ( $n = 29$ ) were described under seven loading conditions: tensile, compression, shear wave ultrasound elastography (SWE), parallel plate rheometry, indentation, creep and relaxation. The EAs displayed a compressive Young's modulus varying from 1.53–16.6 kPa for a percentage strain range of 5%–40%, which was similar to other compressive studies found for human retrieved emboli.<sup>17</sup> The EAs displayed a non-linear response under parallel plate rheometry, creep and stress relaxation. These results have been since validated and published.<sup>26</sup>

Measuring the dimensions of any soft tissue is difficult due to its deformable nature.<sup>27</sup> From literature it is seen that a Vernier callipers can be used to measure highly porous, unstructured tissues, like bovine EAs. EAs, with an average length of  $7.60 \pm 1.00$  mm and average diameter of  $3.82 \pm 0.98$  mm, were measured by an electronic digital Vernier calliper (Maplin, England) with an accuracy of 0.01 mm. Each sample was measured three times to give a fair reliability measurement of the EA<sup>27</sup> and reduce human error.

Two Cameras (50-Hz frame rate, 12 MP) were used to monitor EA trajectories. A flexible connector allowed clots to be released from the left, right and anterior positions. EAs were released at the beginning of each cardiac cycle through a primed, three-way connector. This connector was capable of releasing the EAs from the left, right and anterior positions within the ascending aorta. A total of 240 EAs were released into the physiological simulation system under normal (60 EAs) and AF (180 EAs) pulsatile flow conditions.

### Flow rates replication

The replication of normal ascending aorta flow rates was based upon previously published data.<sup>28</sup> The graph

was scanned and digitised using MATLAB v 7.0.1 (MathWorks, USA). The data points (in Cartesian coordinates) for each graph were extracted at 0.01-s intervals from the scanned image and a smoothing spline applied to these points using the CF TOOL feature within MATLAB. This smoothing was necessary to remove artefacts of pixilation during the digitisation process. The result is a smooth velocity profile under normal physiological flow conditions (Figure 2(a)–solid grey line). The CO was  $7.5 \text{ L min}^{-1}$  with a CL of 0.8 s.

A scaling factor was applied to the healthy profile based on the raw haemodynamic data recorded by Clark et al.<sup>2</sup> (Figure 2(b)–(f)–solid grey line). AF patient velocity profiles are difficult to come by for engineering research. The physical assumption behind applying a scale factor to reproduce the pathological flow curve from a healthy one was also applied in computational studies.<sup>19</sup> Clark et al.<sup>2</sup> shows clear clinical data that we can use to deduce AF parameters and apply to healthy data to obtain useful engineering data. Clark et al.<sup>2</sup> resulted that an irregular sequence of RR intervals produces adverse hemodynamic consequences such as a reduced CO and CL that are independent of heart rate which is agreement with other AF studies.<sup>10,11,29,30</sup>

The scaling factor applied similar to that applied by Choi et al.<sup>19</sup> and displays a CO of  $5 \text{ L min}^{-1}$  in a period of 0.48 s. Four more AF pulsatile flows were also created (Figure 2(c)–(f)–solid grey line). For two of these cases, the pulse period was maintained at 0.48 s and CO was decreased and increased to  $3 \text{ L min}^{-1}$  (Figure 2(c), AF1) and  $7 \text{ L min}^{-1}$  (Figure 2(d), AF2), respectively. CO was maintained at  $5 \text{ L min}^{-1}$  for the other two cases, and pulse period was decreased and increased to 0.4 (Figure 2(e), AF3) and 0.8 s (Figure 2(f), AF4), respectively.

The surrogate blood fluid was a mixture, by weight, of 60% deionised water and 40% glycerine (Vegetable Glycerine, 99.5% min glycerine (E 422), Univar Ltd., West Yorkshire, United Kingdom). The viscosity of the fluid mixture was 3.7 mPas, at a temperature of 21.1 °C, as measured using a cone and plate viscometer (Brookfield DV-II + Pro, USA), connected to a temperature-controlled bath. The standard error of the machine was 1%. Non-Newtonian effects were ignored, as the flow was travelling into large size vessels. Larger vessels allow for a high shear rate at the wall thus displaying Newtonian effects. The fluid was pumped through the aortic arch model in a closed-loop system.

Two ultrasonic flow meters (25-PXL flowsensor; 16-PXL Clamp-on flowsensor, Transonic, USA) were utilised to measure and monitor inlet and outlet flow rates (Figure 2(a)–(f)–dashed grey line). Table 1 displays the recorded average (and percentage) flow rates for the inlet and outlet vessels. The flowsensors had a resolution of  $1 \text{ mL min}^{-1}$  for a scale of  $\pm 25 \text{ L min}^{-1}$  for steady and pulsatile flows. The 25-PXN and 16-PXL ultrasonic inline flowmeters were calibrated for the

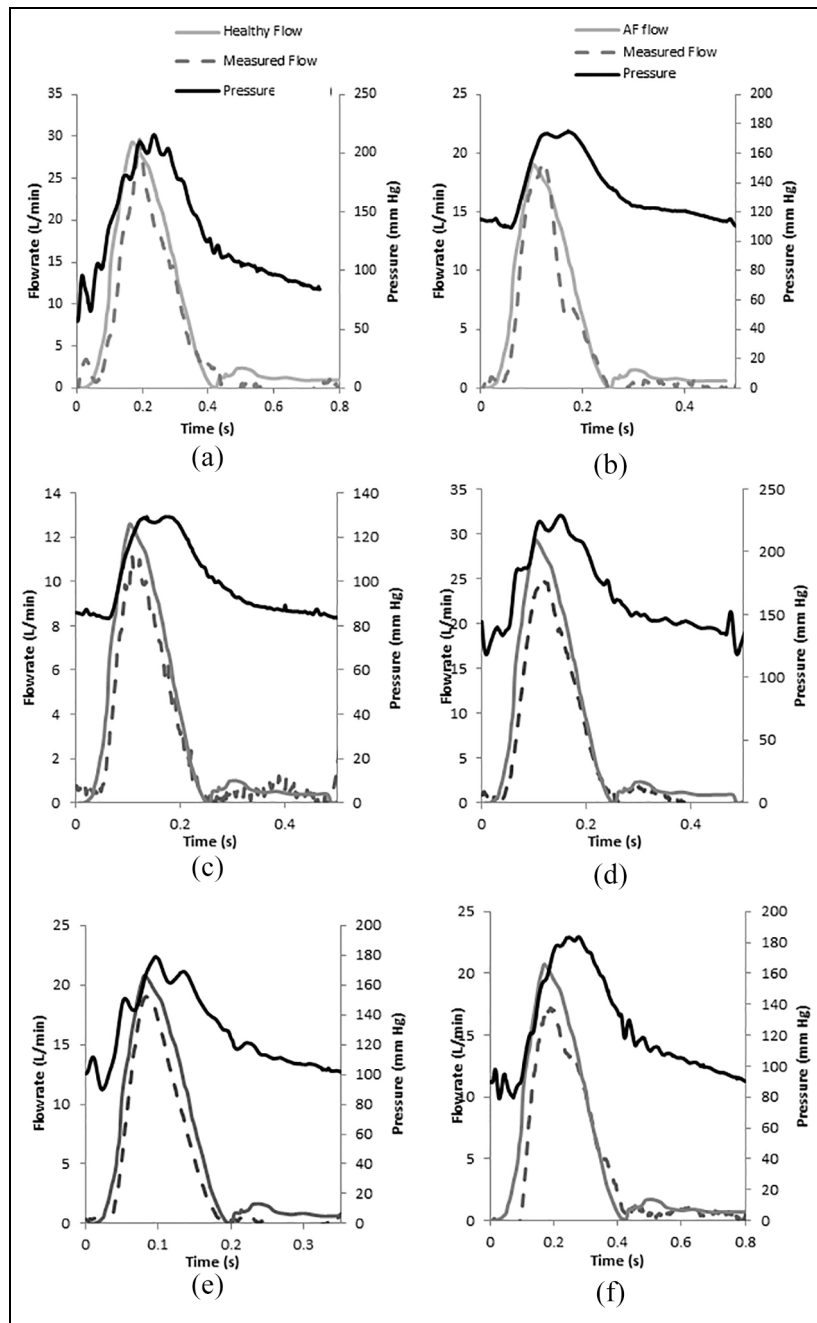


**Figure 2.** Velocity profiles (inputted – solid grey line, measured – dashed grey line) and pressure (black line) profiles for (a) healthy flow, (b) AF average, (c) AF1, (d) AF2, (e) AF3 and (f) AF4.

60:40 of water:glycerine mixture by weight. This calibration was completed using timed (20 s) steady flow collections of the mixture in a graduated cylinder. Each recorded voltage was plotted on a graph with its accompanying flow rate values. This resulted in a linear fit relationship. There was good correlation between desired and measured flow rates as seen in Figure 2.

The pressure within the physiological simulation system was monitored and maintained within physiological ranges with a pressure transducer and an indicator box (Model FDW; R.D.P Electronics Ltd, Sole, United Kingdom) (range: 30 PSIG) (Figure 2(a)–(f)– solid black line). The pressure transducer was calibrated

individually using a varying head height via a head tank. The static head height was adjusted by raising and lowering the head tank. The head pressure ranged from 0 to 140 mmHg. There was a linear relationship between pressure and voltage along the pressure range. As the transducers were prone to drift over time, they were constantly calibrated and recalibrated throughout the experimental work.

#### Flow rate waveform equations

The measured flow rates were fitted with the Fourier series trigonometric fit given by

$$f(t) = \frac{a_0}{2} + \sum_{j=1}^n a_1 \cos(j\omega t) + \sum_{j=1}^n a_1 \sin(j\omega t) \quad (1)$$

where  $a_0, a_1, b_1, a_2, b_2, \dots, a_n, b_n$  are the Fourier series coefficients;  $\omega = (2\pi/T)$ ;  $T$  is the pulse period; and  $n$  is the number of harmonics

The method of least squares was used to obtain the best fit coefficient values using a subroutine written in MATLAB.

The input velocity profiles ( $u(r, t)$ ) across a vessel can be represented by Womersley's solutions for each harmonic of sinusoidal flow within a straight tube<sup>31</sup> given by

$$u(r, t) = \frac{ikR^2}{\mu\alpha^2} \left( 1 - \frac{J_0(\zeta)}{J_0(\Lambda)} \right) e^{i\omega t} \quad (2)$$

The oscillatory flow rate  $Q(t)$  is found by integrating the oscillatory velocity profile over a cross section giving

$$Q(t) = \int_0^r 2\pi r u(r, t) dr = \frac{i\pi k R^2}{\mu\alpha^2} \left( 1 - \frac{2J_1(\zeta)}{\Lambda J_0(\Lambda)} \right) e^{i\omega t} \quad (3)$$

where  $\alpha = R\sqrt{(\rho\omega/\mu)}$ ;  $\Lambda$  is a complex frequency parameter given by  $((i-1)/\sqrt{2})\alpha$ ;  $\zeta$  is a complex variable related to the radial coordinate  $r$  and is given by  $\Lambda(r/R)$ ;  $J_0$  and  $J_1$  are Bessel functions zero and first order, respectively; and  $k$  is the oscillatory pressure gradient.

To incorporate equation (1) for a physiological flow rate waveform as described by the Fourier series curve fits, a Womersley solution would be obtained for each harmonic with corresponding coefficients  $a_1, b_1, a_2, b_2, \dots, a_n, b_n$  and summed together. The Fourier series coefficients represent the amplitude of the oscillatory flow rates at each harmonic. These summed harmonic solutions would then be added to the steady state solution as given by Poiseuille flow as defined by the steady state coefficient  $a$  and summed together. The Fourier series coefficients represent the amplitude of the oscillatory flow rates at each harmonic. These summed

harmonic solutions would then be added to the steady state solution as given by Poiseuille flow as defined by the steady state coefficient  $a_0/2$ , which is the amplitude of the steady flow rate.

### Statistical analysis

The  $\chi^2$  test was used to test the hypotheses whether EA trajectories are distributed proportionally to flow rate type. In all cases, the experimental data were compared to the null hypothesis (uniform distribution of EAs) using a simple  $\chi^2$  goodness-of-fit test within Minitab 17.0 (Minitab Inc. State College, PA, USA). The authors declare that all supporting data are available within the article.

A power analysis was completed using statistical software (R, R Core Team 2013, Version 4.0) to determine the probability of detecting an effect of a given size with a given level of confidence, under a certain sample size. If the probability is unacceptably low, it would be wise to alter or abandon the experiment. Using a chi-square power calculation and a medium effect size of 0.3,<sup>32</sup> a power value of 0.967 was calculated, showing that the hypothesis test is a very good at detecting a false null hypothesis. It must be noted that the sample size in this experimental design is governed by the availability of fresh blood clot specimens for testing and the length of time required to execute one test. One test scenario took between 5 and 10 min to release, record, remove and prepare for the next test. The physiological simulation system then required intensive cleaning to remove clots from the system at the beginning and the end of every day. To execute 240 clots as in this study, required 10 h of solid testing for 10 days with fresh clot preparation carried out throughout.

### Results

Table 2 displays the number of clots that travelled through the outlet vessels under healthy and AF flow conditions ( $n = 240$ ) when released from the left (L), right (R) and anterior (A) positions. Under healthy flow conditions ( $n = 60$ ), the EAs tended to follow the flow rate split through each outlet vessel. A total of 10% of EAs travelled through the LCCA and right common carotid artery (RCCA), leading towards the

**Table 1.** Average flow rates along each vessel, under six different flow conditions: healthy, AF and AFI-4.

| Vessel           | Healthy (%) | AF datum (%) | AF1 (%)   | AF2 (%)   | AF3 (%)   | AF4 (%)   |
|------------------|-------------|--------------|-----------|-----------|-----------|-----------|
| Ascending aorta  | 7200        | 5000         | 3000      | 7000      | 5000      | 5000      |
| Right subclavian | 500 (7)     | 400 (8)      | 250 (8)   | 500 (7)   | 400 (8)   | 400 (8)   |
| Right CCA        | 400 (6)     | 300 (6)      | 200 (7)   | 400 (6)   | 300 (6)   | 300 (6)   |
| Left CCA         | 400 (6)     | 300 (6)      | 200 (7)   | 400 (6)   | 300 (6)   | 300 (6)   |
| Vas              | 100 (1)     | 100 (1)      | 50 (1)    | 100 (1)   | 100 (1)   | 100 (1)   |
| Left subclavian  | 500 (7)     | 400 (8)      | 200 (7)   | 500 (7)   | 400 (8)   | 400 (8)   |
| Descending aorta | 5300 (74)   | 3500 (70)    | 2100 (70) | 5000 (73) | 3500 (70) | 3500 (70) |

AF: atrial fibrillation; CCA: common carotid artery.



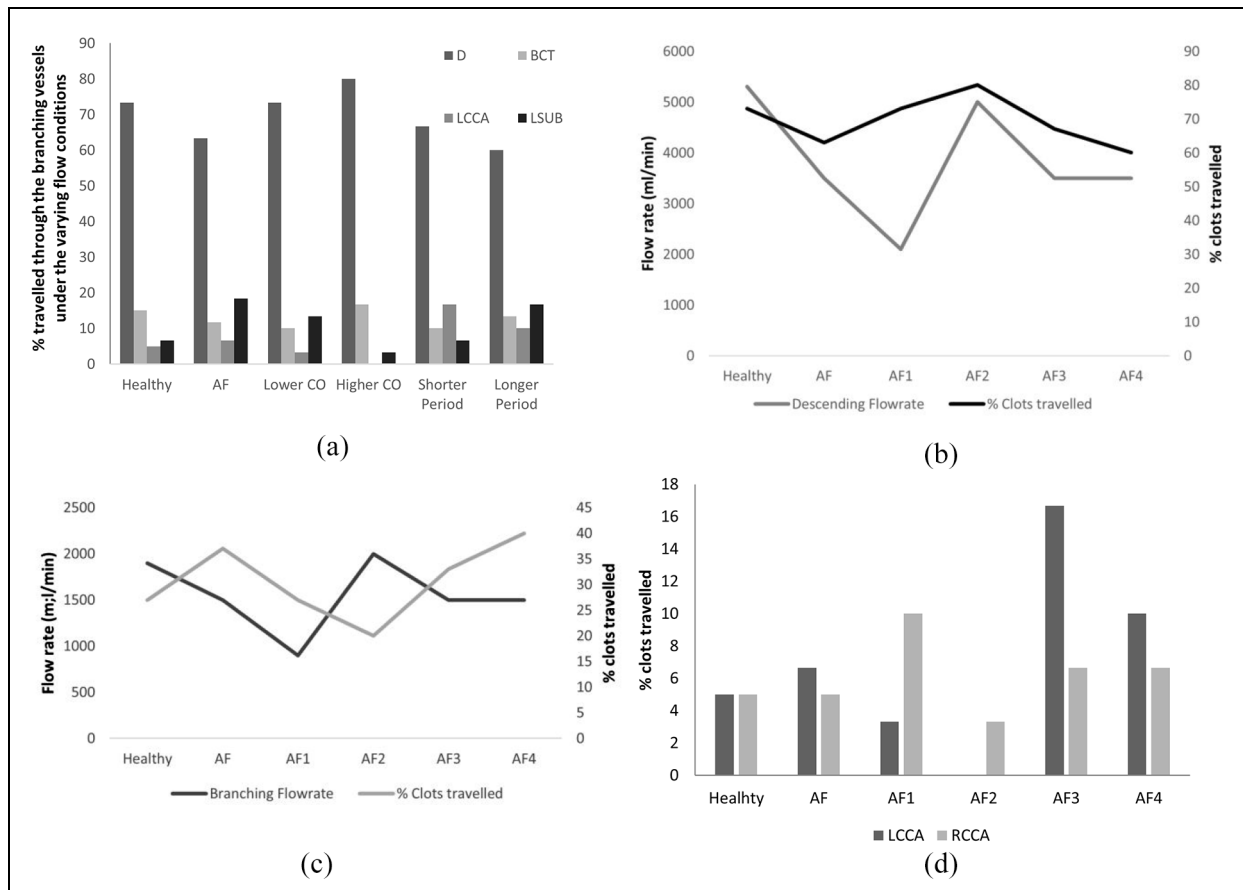


**Figure 3.** (a) Bar chart of the % clots that travelled through the branching vessels under varying flow conditions; (b) trend line displaying the relationship between descending aorta flow rate and % clot trajectories; (c) trend line displaying the relationship between branching vessels aorta flow rate and % clot trajectories; and (d) bar chart displaying the % clots that travelled through the common carotid arteries.

**Table 3.** The coefficient values for a 10 harmonic Fourier series trigonometric fit for each measured input flow rate.

| Coefficients | Healthy | AF      | AF1     | AF2     | AF3     | AF4     |
|--------------|---------|---------|---------|---------|---------|---------|
| $a_0$        | 5.7667  | 2.5634  | 2.5644  | 5.8796  | 3.4942  | 3.9624  |
| $a_1$        | -5.3993 | -0.5063 | -0.6023 | -0.8647 | -0.9365 | -2.2689 |
| $b_1$        | 8.1956  | 3.7519  | 3.7374  | 9.0135  | 6.551   | 6.3914  |
| $a_2$        | -2.7765 | -2.6232 | -2.5922 | -5.8848 | -4.3301 | -3.8048 |
| $b_2$        | -4.8376 | -0.4836 | -0.6202 | -0.2655 | -0.8325 | -1.5045 |
| $a_3$        | 2.6713  | 0.156   | 0.2416  | -0.1033 | 0.272   | 0.3322  |
| $b_3$        | -0.5205 | -1.0715 | -1.056  | -2.9439 | -2.6734 | -1.7236 |
| $a_4$        | 0.3711  | 0.5315  | 0.5601  | 0.6348  | 1.1173  | 0.9494  |
| $b_4$        | 1.5329  | -0.2825 | -0.2255 | -1.0496 | -0.1946 | -0.5222 |
| $a_5$        | -0.9061 | 0.4357  | 0.4071  | 0.9977  | 0.7328  | 0.8683  |
| $b_5$        | 0.1796  | 0.2062  | 0.2612  | -0.0269 | 0.6567  | 0.284   |
| $a_6$        | -0.515  | 0.0428  | 0.0065  | 0.1661  | -0.0621 | -0.0016 |
| $b_6$        | -0.7453 | 0.2419  | 0.2455  | 0.4771  | 0.6508  | 0.7907  |
| $a_7$        | 0.6829  | -0.0937 | -0.1157 | -0.1178 | -0.19   | -0.2278 |
| $b_7$        | 0.0612  | 0.1406  | 0.121   | 0.2535  | 0.0437  | 0.2761  |
| $a_8$        | -0.1809 | -0.06   | -0.0662 | -0.0808 | -0.1214 | -0.1734 |
| $b_8$        | -0.3161 | 0.0457  | 0.0321  | 0.0294  | -0.082  | -0.1108 |
| $a_9$        | 0.3532  | -0.0381 | -0.0341 | 0.0098  | -0.0725 | -0.1179 |
| $b_9$        | -0.234  | -0.004  | -0.0129 | 0.1423  | 0.0046  | 0.0737  |
| $a_{10}$     | 0.3029  | -0.0138 | 0       | 0.0182  | -0.0129 | -0.081  |
| $b_{10}$     | 0.2636  | -0.0434 | -0.0456 | 0.0274  | 0.0128  | -0.1282 |

AF: atrial fibrillation.

increase in atrial pressure and a reduced interval for diastolic filling.<sup>2,10,11,29,30</sup> These effects are also likely to vary among patients. The independent effects of varying CO and pulse period were analysed and compared to healthy, regular pulsatile flow. Pressure was higher in flows with a higher CO and longer pulse period (0.8 s).

In total, 240 bovine EAs were fabricated for this study. The purpose of the bovine EAs was to simulate the trajectory paths of cardiac source clots. The mechanism of coagulation is universal across mammalian biology.<sup>34</sup> Ovine, porcine and bovine blood is the most frequently used mammalian blood for EA replication.<sup>17,26,35–38</sup> Bovine blood was chosen for EA manufacture as the supply was in close proximity to the laboratory (Burkes Abattoir Ltd, Galway, Ireland) and also, on a macro level, the composition of bovine blood is similar to human.<sup>39</sup>

Our results show that for all conditions, the number of clots (with an average length of  $7.60 \pm 1.00$  mm and average diameter of  $3.82 \pm 0.98$  mm) travelling through the varying branches was proportional to the flow rate. The results showed that 25%–35% of EAs travelled along the branching vessels for all tests. This percentage of EAs was proportional to the percentage flow rate split of 25%–31% along the branching vessels. The descending outlet flow rate was 74% of the overall flow rate and 73% EAs travelled through the descending aorta. Chung et al.<sup>13</sup> showed that the distribution of smaller emboli approaches proportionality with flow, while larger diameter emboli (1000  $\mu$ m) travel along the vessel with the greatest flowrates.<sup>13</sup> Bushi et al.<sup>12</sup> studied emboli trajectory patterns through Y-shaped bifurcation models and showed large spherical particles, of diameters 0.6, 1.6 and 3.2 mm, preferentially entering the wider bifurcation branch. There are similar bifurcations and movement of clots within our model; however, the rigid vessel diameters used in these studies<sup>12,13</sup> were of a much smaller diameters than ours. The Y model employed in Bushi et al.<sup>12</sup> displayed diameters of 4 and 6 mm. Chung et al.<sup>13</sup> used a cerebral model ranging in diameters from 1.7 to 6.1 mm. Table 4 displays the measured diameters of the aortic arch model in our experimental work.

Carr et al.<sup>18</sup> demonstrated computationally that cardiogenic emboli appeared to have a strong

size-destination relationship, varying from previous research expectations that blood clot distribution should generally favour arteries that receive the highest volumetric blood flow. This study is the closest to ours in design; however, there are some key differences. The embolus model used in the computation is spherical in shape which denotes a lower drag force than the biologically comparable EA used in our physiological simulation system. Blood clots have been shown to display different properties in different directions and different loading conditions<sup>26</sup> and this, along with the geometry of the clot, effects the mobility of the clot during trajectory in a different way to a sphere. The clot has the ability to compress, stretch and deform to fit into vessels that might not be intuitively obvious. Malone et al.<sup>15</sup> showed that clots up to 6 mm in diameter and over 30 mm in length can travel through the narrower vessels of the cerebral vasculatures. The bovine EAs displayed a compressive Young's modulus of 7 kPa (5% strain) to 84 kPa (50% strain) which is magnitudes lower than the model employed by Carr et al.,<sup>18</sup> which was based on an intraluminal thrombus model.<sup>40</sup> This model did not display a visco-elastic response as seen in biological clots. It should also be noted that the blood pressure in the computational work was undocumented and therefore difficult to compare fully with our experimental work.

Under AF flow conditions ( $n = 180$ ), the percentage of EAs travelling through the descending aorta decreased to an average of 68%. Subsequently, EA trajectories increased under AF pulsatile flow conditions through the carotid arteries and subclavian arteries from 10% to 13% and 17% to 19%, respectively. The in vitro simulation demonstrates that AF increases the number of EAs to travel through the branching vessels from the aortic arch. Choi et al. showed numerically that the reduced CO and CL induced by AF can significantly increase the incidence of carotid embolisation. In our study, all AF flows displayed a higher propensity for carotid embolisation except AF2. This was due to the higher CO ( $7 \text{ L min}^{-1}$ ) which was similar to the healthy flow CO ( $7.2 \text{ L min}^{-1}$ ). This higher CO tends to manipulate clot trajectory paths towards the descending aorta. Our study has experimentally confirmed that there was an increase in stroke propensity for AF3,  $\chi^2(1, N = 90) = 6.945$ ,  $p < 0.05$ . AF3 had a shorter period (0.3 s) than the scaling factor used by Choi et al. The reduced CO and shorter period resulted in the greatest number of EAs travelling through the LCCA and RCCA vessels. It also resulted in 'fluttering' of the EAs within the CCA vessels. This occurred in 3% of tests, where the EA remained within the carotid vessel(s) for a substantial period of time before eventually passing fully through the vessel to the cerebral vasculature. Although 60% EAs travelled through the descending aorta under AF4, which was the lowest of all six flows, the majority of EAs travelled through the left subclavian and not the carotid arteries.

**Table 4.** Measured diameters of the aortic arch model.

| Vessel      | Diameter (mm)    |
|-------------|------------------|
| Aortic arch | $27.27 \pm 2.62$ |
| BCT         | $14.64 \pm 0.52$ |
| R sub       | $11.17 \pm 2.62$ |
| RCCA        | $8.01 \pm 0.38$  |
| LCCA        | $7.63 \pm 0.92$  |
| L sub       | $10.49 \pm 0.73$ |

BCT: brachiocephalic trunk; RCCA: right common carotid artery; LCCA: left common carotid artery.



Left–right propensity of stroke inducing cardiogenic emboli is a conflicting topic in the literature. Meyer et al.<sup>41</sup> showed that more embolisation (64%) occurred through the LCCA, while only 31% of emboli entered through the RCCA. It is not shown in Meyer's study whether the data recorded was from AF patient cases. Cardiogenic emboli have been observed to have right brain propensity, due to the first vessel branching from the aortic arch being the RCCA.<sup>42–44</sup> Other clinical data suggest left hemisphere strokes are more common than right hemisphere strokes, as cardioembolic ischemic strokes in the left middle cerebral artery (MCA) are more frequent due to vessel thickness and geometry.<sup>19,45,46</sup> Differences have also been detected in the number and size of left and right ischemic lesions.<sup>47</sup>

In our study, the number of embolisations that occurred through the LCCA (16 EAs, 7%) compared to the RCCA (14 EAs, 6%) was almost 50:50. More RCCA embolisations occurred under AF1 and AF2 flow conditions. The recorded outlet flow rates through the model LCCA and RCCAs were kept equal and therefore the tendency for EAs to travel through the LCCA or RCCA could be attributed to aortic arch branching and location. The BCT did experience the most trajectories probably because it branches first from the aortic arch, in agreement with previous work.<sup>42–44</sup> However, variations in branching in aortic arch models would allow for future studies to fully understand this relationship between RCCA and LCCA propensity in stroke occurrence and arch geometry.

The 77-year-old AF patient-case had a distal occlusion of the right M1 vessel, which would indicate a blood clot trajectory through the RCCA under similar physiological conditions as AF1 or AF2. The risk of cardiogenic embolism can vary within the patient's individual cardiac abnormalities, including but not limited to heart disease, age, duration of arrhythmia, chronic versus intermittent fibrillation and atrial size.<sup>48</sup> It is quite possible that the presence of a possible cardiac source of embolism does not necessarily mean that the stroke was caused by an embolus from the heart under these conditions. Simultaneous atherosclerosis of the CCAs is another common cause of stroke in such patients.<sup>49</sup> However, the data set obtained is a good foundation for the investigation into cardio embolic stroke.

Reducing CO and CL is not the only representative haemodynamic factors in AF. AF is also characterised by irregular heartbeats<sup>2</sup> which may lead to a variety of cardiac hemodynamic profiles. Further studies are necessary to understand the full role of AF haemodynamics in embolic trajectory paths.

## Conclusion

An experimental flow rig was designed and developed for in vitro testing of normal and AF pulsatile flow and

pressure conditions through a compliant, patient-specific, aortic arch model. In order to experimentally reproduce AF flow conditions, a normal, healthy velocity profile was scaled down using measured cardiovascular data from AF patients. Under healthy flow conditions, the clots tended to follow the outlet flow rate splits. AF flow rates increased the probability of a clot travelling along the common carotid arteries, thus increasing the possibility of stroke occurrence.

## Declaration of conflicting interests

The author(s) declared no potential conflicts of interest with respect to the research, authorship and/or publication of this article.


## Ethical approval

The ethics committee waived the need for patient consent.

## Funding

The author(s) disclosed receipt of the following financial support for the research, authorship and/or publication of this article: Galway Mayo Institute of Technology 40th anniversary seed funding.

## ORCID iD

Fiona Malone  <https://orcid.org/0000-0001-7917-1854>

## Supplemental material

Supplemental material for this article is available online.

## References

1. Waktare JEP. Atrial fibrillation. *Circulation* 2002; 106: 14–16.
2. Clark DM, Plumb VJ, Epstein AE, et al. Hemodynamic effects of an irregular sequence of ventricular cycle lengths during atrial fibrillation. *J Am Coll Cardiol* 1997; 30: 1039–1045.
3. Kelly-Hayes M. Influence of age and health behaviors on stroke risk: lessons from longitudinal studies. *J Am Geriatr Soc* 2010; 58: 325–328.
4. Fuster V, Ryden LE, Cannom DS, et al. Guidelines for the management of patients with atrial fibrillation. *Circulation* 2006; 114: 257–354.
5. Heeringa J, Van der Kuip DA, Hofman A, et al. Prevalence, incidence and lifetime risk of atrial fibrillation: the Rotterdam study. *Eur Heart J* 2006; 27: 949–953.
6. Menke J, Lüthje L, Kastrup A, et al. Thromboembolism in atrial fibrillation. *Am J Cardiol* 2010; 105: 502–510.
7. Wolf PA, Abbott RD and Kannel WB. Atrial fibrillation as an independent risk factor for stroke: the Framingham study. *Stroke* 1991; 22(8): 983–988.
8. Phillips SJ. Is atrial fibrillation an independent risk factor for stroke? *Can J Neurol Sci* 1990; 17: 163–168.

9. Chesebro JH, Fuster V and Halperin JL. Atrial fibrillation: risk marker for stroke. *N Engl J Med* 1990; 323: 1556–1558.
10. Nathanakumar K and Kay GN. The deleterious effects of an irregular RR interval. *Eur Heart J* 2002; 23: 695–696.
11. Popovic ZB, Mowrey KA, Zhang Y, et al. Slow rate during AF improves ventricular performance by reducing sensitivity to cycle length irregularity. *Am J Physiol Heart Circ Physiol* 2002; 283: H2706–H2713.
12. Bushi D, Grad Y, Einav S, et al. Hemodynamic evaluation of embolic trajectory in an arterial bifurcation: an in vitro experimental model. *Stroke* 2005; 36: 2696–2700.
13. Chung EML, Hague JP, Chanrion MA, et al. Embolus trajectory through a physical replica of the major cerebral arteries. *Stroke* 2010; 41: 647–652.
14. Fahy P, Malone F, McCarthy E, et al. An in vitro evaluation of emboli trajectories within a three-dimensional physical model of the circle of Willis under cerebral blood flow conditions. *Ann Biomed Eng* 2015; 43(9): 2265–2278.
15. Malone F, McCarthy E, Delassus P, et al. Investigation of the hemodynamics influencing emboli trajectories through a patient-specific aortic arch model. *Stroke* 2019; 50: 1531–1538.
16. Malone F, McCarthy E, Delassus P, et al. Embolus analog trajectory paths under physiological flowrates through patient-specific aortic arch models. *J Biomech Eng* 2019; 141(10): 101007.
17. Chueh JK, Wakhloo AK, Hendricks GH, et al. Mechanical characterisation of thromboemboli in acute ischemic stroke and laboratory embolus analogs. *Am J Neuroradiol* 2011; 32: 1237–1244.
18. Carr IA, Nemoto N, Schwartz RS, et al. Size-dependent predilections of cardiogenic embolic transport. *Am J Physiol Heart Circ Physiol* 2013; 305(5): H732–H739.
19. Choi HW, Navia JA and Kassab GS. Stroke propensity is increased under atrial fibrillation hemodynamics: a simulation study. *PLoS ONE* 2013; 8: e73485.
20. Ou P, Celermajer DS, Mousseaux E, et al. Vascular remodeling after ‘successful’ repair of coarctation: impact of aortic arch geometry. *J Am Coll Cardiol* 2007; 49(8): 883–890.
21. Demertzis S, Hurni S, Stalder M, et al. Aortic arch morphometry in living humans. *J Anat* 2010; 217(5): 588–596.
22. Fahy P, McCarthy P, Sultan S, et al. An experimental investigation of the hemodynamic variations due to aplastic vessels within three-dimensional phantom models of the circle of Willis. *Ann Biomed Eng* 2013; 42(1): 123–138.
23. Raghavan ML, Kratzberg J, Castro de Tolosa EM, et al. Regional distribution of wall thickness and failure properties of human abdominal aortic aneurysm. *J Biomech* 2006; 39(16): 3010–3016.
24. Thubrikar M, Labrosse MR, Robicsek F, et al. Mechanical properties of abdominal aortic aneurysm wall. *J Med Eng Technol* 2000; 25: 133–142.
25. Di Martino ES, Bohra A, Vande Geest JP, et al. Biomechanical properties of ruptured versus electively repaired abdominal aortic aneurysm wall tissue. *J Vasc Surg* 2006; 43: 570–576.
26. Malone F, MacCarthy E, Delassus P, et al. The mechanical characterisation of bovine embolus analogues under various loading conditions. *Cardiovasc Eng Technol* 2018; 9: 489–502.
27. O’Leary SA, Doyle BJ and McGloughlin TM. Comparison of methods used to measure the thickness of soft tissues and their influence on the evaluation of tensile stress. *J Biomech* 2013; 46(11): 1955–1960.
28. Reymond P, Merenda F, Perren F, et al. Validation of a one-dimensional model of the systemic arterial tree. *Am J Physiol Heart Circ Physiol* 2009; 297: H208–H222.
29. Daoud EG, Weiss R, Bahu M, et al. Effect of an irregular ventricular rhythm on cardiac output. *Am J Cardiol* 1996; 78: 1433–1436.
30. Lee DC, Markl M, Ng J, et al. Three-dimensional left atrial blood flow characteristics in patients with atrial fibrillation assessed by 4D flow CMR. *Eur Heart J Cardiovasc Imaging* 2016; 17(11): 1259–1268.
31. Zamir M. *The physics of pulsatile flow*. 1st ed. New York: Springer-Verlag Inc., 2000.
32. Cohen J. *Statistical power analysis for the behavioral sciences*. Hillsdale, NJ: Lawrence Erlbaum Associates, 1988.
33. Uflacker R. *Atlas of vascular anatomy: an angiographic approach*. 2nd ed. Charleston, SC: Lippincott Williams & Wilkins, 2007.
34. Davie EW and Fujikawa K. Basic mechanisms in blood coagulation. *Annu Rev Biochem* 1975; 44: 799–829.
35. Duffy S, Farrell M, McArdle K, et al. Novel methodology to replicate clot analogs with diverse composition in acute ischemic stroke. *J Neurointerv Surg* 2016; 9: 486–491.
36. Robinson RA, Herbertson LH, Sarkar Das S, et al. Limitations of using synthetic blood clots for measuring in vitro clot capture efficiency of inferior vena cava filters. *Med Devices* 2013; 6: 49–57.
37. Krasokha N, Theisen W, Reese S, et al. Mechanical properties of blood clots – a new test method. *Materialwiss Werkst* 2010; 41: 1019–1024.
38. Schmitt C, Henni AH and Cloutier G. Characterization of blood clot viscoelasticity by dynamic ultrasound elastography and modeling of the rheological behaviour. *J Biomech* 2011; 44: 622–629.
39. Stone WH. The relation of human and cattle blood groups. *Transfusion* 1962; 2(3): 172–177.
40. Wang DH, Makaroun M, Webster MW, et al. Mechanical properties and microstructure of intraluminal thrombus from abdominal aortic aneurysm. *J Biomech Eng* 2001; 123(6): 536–539.
41. Meyer JS, Charney JZ, Rivera VM, et al. Cerebral embolization: prospective clinical analysis of 42 cases. *Stroke* 1971; 2(6): 541–554.
42. Mukherjee D, Jani ND, Selvagesan K, et al. Computational assessment of the relation between embolism source and embolus distribution to the circle of Willis for improved understanding of stroke etiology. *ASME J Biomech Eng* 2016; 138(8): 081008.
43. Park KY, Kim YB, Chung PW, et al. Right-side propensity of cardiogenic emboli in acute ischemic stroke with atrial fibrillation. *Scand Cardiovasc J* 2014; 48(6): 335–338.
44. Gold M, Khamesi M, Sivakuma M, et al. Right-left propensity of cardiogenic cerebral embolism in standard versus bovine aortic arch variant. *Clin Anat* 2018; 31(3): 310–313.
45. Hedna WS, Bodhit AN, Ansari S, et al. Hemispheric differences in ischemic stroke: is left hemisphere stroke more common? *J Clin Neurol* 2013; 9(2): 97–102.

46. Rodriguez Hernandez S, Kroon AA, van boztel MPJ, et al. Is there side predilection for cerebrovascular disease? *Hypertension* 2003; 42(1): 56–60.
47. Patel N, Horsfield MA, Banahan C, et al. Impact of peri-operative infarcts after cardiac surgery. *Stroke* 2015; 46(3): 680–686.
48. Leary MC and Caplan LR. Carioembolic stroke: an update on etiology, diagnosis and management. *Ann Indian Acad Neurol* 2008; 11: 52–63.
49. Bogousslavsky J, Van Melle G, Regli F, et al. Pathogenesis of anterior circulation stroke in patients with non-valvular atrial fibrillation: the Lausanne Stroke Registry. *Neurology* 1990; 40: 1046–1050.